This is an *Accepted Manuscript*, which has been through the Royal Society of Chemistry peer review process and has been accepted for publication.

Accepted Manuscripts are published online shortly after acceptance, before technical editing, formatting and proof reading. Using this free service, authors can make their results available to the community, in citable form, before we publish the edited article. We will replace this *Accepted Manuscript* with the edited and formatted *Advance Article* as soon as it is available.

You can find more information about *Accepted Manuscripts* in the **Information for Authors**.

Please note that technical editing may introduce minor changes to the text and/or graphics, which may alter content. The journal's standard **Terms & Conditions** and the **Ethical guidelines** still apply. In no event shall the Royal Society of Chemistry be held responsible for any errors or omissions in this *Accepted Manuscript* or any consequences arising from the use of any information it contains.

Journal Name

ARTICLE

Composite of K-doped (NH₄)₂V₃O₈/graphene as an anode material for sodium-ion batteries

Xin Liu,[a,b] Zhiwei Li[a,b] Hailong Fei,*[a,b] and Mingdeng Wei*[a,b]

A layered structural K-doped (NH₄)₂V₃O₈/graphene (K-NVG) was prepared via a hydrothermal route and then used as an anode material for sodium-ion batteries for the first time. The K-NVG nanosheets have a diameter in the range of 200-500 nm in width. The K-NVG electrode exhibited stable cycling and good rate performance with a reversible capacity of 235.4 mA h g^{-1}, which is much higher than 90.5 mA h g^{-1} of the (NH₄)₂V₃O₈/graphene electrode after 100 cycles at the current density of 100 mA g^{-1}. Simultaneously, the retention rate was maintained at 82% even after 250 cycles at the current density of 300 mA g^{-1}. Such a good electrochemical property may be attributed to the K-NVG's stable layered structure.

Introduction

In recent years, with the increasing concerns about renewable energy sources, low-cost, high power and safety energy-storage devices have attracted much attention.[1-5] Among these devices, although lithium-ion batteries (LIBs) have gained many achievements,[6-7] their limited availability and increasing cost with worldwide commercialization cannot satisfy the substantial demand.[8-9] Meanwhile, sodium, possessing similar physical and chemical properties to lithium, has caused many researchers' interest. The development of Na-ion batteries has many advantages such as almost infinite supply in the earth's crust, low cost and good security.[10-13] To date, great efforts have been made in the design of various electrode materials for SIBs such as Ti-based compounds[14], Na-alloys[15-17] and carbon materials[18-20]. However, they did not exhibit good electrochemical properties. Thus, the development of newly electrode materials for SIBs is essential.

Vanadium oxides and vanadates as important functional materials have been widely investigated for Na-ion batteries due to their abundant source, low cost and high energy density and good electrochemical performance.[21-23] But as a branch of the vanadates, ammonium vanadates have not attracted more studies than other vanadates. We are encouraged to extend our studies on ammonium vanadates. From the past research[24-26], there are two main defects that restrict the application of ammonium vanadates bronzes in sodium-ion batteries. First, due to the instability of NH_4^+, the structure of ammonium vanadates is easily destroyed after repeating sodiation and desodiation. Second, compared with other vanadates,

the capacity of ammonium vanadates is not very high. To overcome the first problem, vanadates and vanadium oxides were often coated with carbon materials. It has been found that the stability of vanadates or vanadium oxides can be obviously improved by compositing with carbon materials.[27-29] Among these carbon materials, graphene, with a flexible structure, superior electrical conductivity and high surface area, has recently attracted much attention in SIBs. For example, Arumugam and his co-workers synthesized VO₂/rGO nanorods which exhibited enhanced electrochemical performance, obviously.[30] Meanwhile, it has been found that doping metal ions in vanadium oxides and vanadates is a good way to solve the second issue.[31-33] For instance, Xu et al.[34] synthesized Ti-doped V₂O₅ which displayed higher capacity than pure V₂O₅. Cao et al.[35] synthesized Mo-doped LiV₃O₈ which capacity is much higher than 97.8 mA h g^{-1} of the pure LiV₃O₈ during the 100th cycle at the current density of 300 mA g^{-1}.

In the present work, the composites of K-doped (NH₄)₂V₃O₈/graphene (K-NVG) were synthesized via a simple hydrothermal route and then used as the anode materials for SIBs for the first time. Compared with the (NH₄)₂V₃O₈, (NH₄)₂V₃O₈/grapheme and some other V-based materials[36, 37] the composites exhibited an obviously improved in long life cycles and capacity. For instance, K-NVG delivered a discharge capacity of 235.4 mA h g^{-1}, which is much higher than 90.7 mA h g^{-1} of (NH₄)₂V₃O₈/graphene (NVG) at the current density of 100 mA g^{-1} during the 100th cycles. Furthermore, after 250 cycles, the K-NVG electrode exhibited a high capacity of 142 mA h g^{-1} at the current density of 300 mA g^{-1}.

Experimental

Synthesis of K-doped (NH₄)₂V₃O₈

The graphene oxide (GO) was synthesized from natural graphite flakes by a modified Hummers method.[38] The K-NVG was synthesized by a simple hydrothermal method. In a typical synthesis, 0.4 g NH₄VO₃ and different amounts of KNO₃ (molar ratio K:

[a.] State Key Laboratory of Photocatalysis on Energy and Environment, Fuzhou University, Fuzhou, Fujian 350002, China.
[b.] Institute of Advanced Energy Materials, Fuzhou University, Fuzhou, Fujian 350002, China; E-mail: fimer@126.com (H.L. Fei), wei-mingdeng@fzu.edu.cn (M.D. Wei).
† Electronic Supplementary Information (ESI) available: [details of any supplementary information available should be included here]. See DOI: 10.1039/x0xx00000x

V=0%, 5% and 10%) were dissolved in 35 ml ethanol under intense agitation, and then 15 mg GO was added into the above solution. After stirring for 2 hours, the resulting solution was poured into a Teflon-lined stainless-steel autoclave with a 50 ml capacity and heated at 180 °C for 24 hours. After being cooled to room temperature, the resulting black precipitate was separated by centrifugation and washed by ethanol several times. Finally, the products were dried at 60 °C overnight under air. Herein, the K-NVG materials prepared with different amounts of KNO_3 are denoted as K-0, K-1 and K-2, respectively.

Structural and elemental characterization

X-ray diffraction (XRD) patterns were recorded on PANalytical X'Pert spectrometer using the Co-Kα radiation and the data were changed to Cu- Kα data. Scanning electron microscopy (SEM) and transmission electron microscopy (TEM) were taken on a Hitachi S4800 instrument and a FEI S-TWIN instrument, respectively. Raman spectroscopy was performed on a microscopic confocal Laser Raman Spectrometer (inVia Reflex, Renishaw Co.) using a 532 nm laser at room temperature.

Electrochemical measurements

To evaluate the electrochemical performance, the working electrode was constructed by mixing the active material, acetylene black (AB) powder and polyvinylidene fluoride (PVDF) powder in a weight ratio of 70: 20: 10. The mixture was added to N-methyl-2-pyrrolidinone solvent to form homogeneous slurry and pressed on Cu foil circular flakes, and then dried at 90 °C overnight under vacuum conditions. The electrolyte was 1 M $NaClO_4$ in a 1: 1: 1 (volume ratio) mixture of ethyl-carbonate (EC), ethyl methyl carbonate (EMC) and dimethyl carbonate (DMC). The cells were assembled in a glove box filled with highly pure argon gas, and charge–discharge tests were performed in the voltage range of 0.05 to 3 V (Na^+/Na) on a Land automatic battery tester (Land CT 2001A, Wuhan,China). The electrochemical impedance spectroscopy (EIS) was performed on an IM6 Electrochemical Workstation (Zahner). The EIS data were collected with an AC voltage of 10 mV amplitude in the frequency range from 1 mHz to 100 mHz.
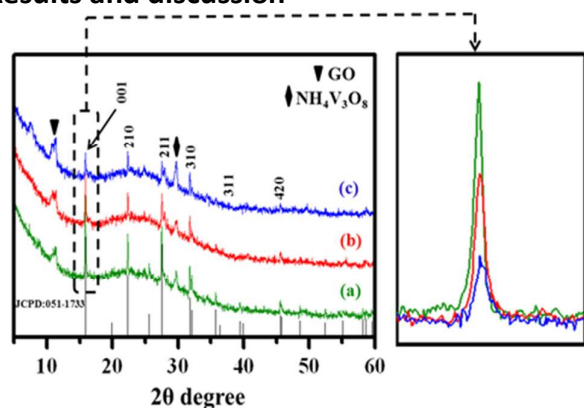
.

Results and discussion

Fig. 1 XRD patterns of K-doped $(NH_4)_2V_3O_8$/graphene materials (a) K-0, (b) K-1 and (c) K-2.

Fig. 1 shows the XRD patterns of the K-doped $(NH_4)_2V_3O_8$/graphene samples. All the diffractions can be indexed to the tetragonal $(NH_4)_2V_3O_8$ (JCPDS No. 51-1733, space group: P4bm). At the same time, the $(NH_4)_2V_3O_8$ has been proved that possess layered structure by some reports.[39-41] The diffractions peaks at 10 and 30 degrees demonstrates that little graphene oxide and $NH_4V_3O_8$ phases appear in the final products. However, the doping amount of KNO_3 is limited. When the molar ratio of K to V more than 12.5%, the final product will change to $(NH_4)_{1.92}V_3O_8$ phase (Fig. S1). First, all the diffraction peaks of the JCPDS: 00-37-0515 appeared before 45 degree. This is same to ours. Second, the strongest diffraction peak of JCPD: 51-1733 is (001). However, (001), (120), (121) are the strongest diffractions of JCPD: 00-37-0515. The peak of 28 degree in Fig.S1 belongs to $(NH_4)_2V_3O_8$. As is well known, the formation of ammonium vanadates is strongly dependent on pH value and addition agents.[25, 26] Simultaneously, the differences between them were also observed from the main pattern. With the increasing KNO_3 amount, the intensity of diffraction peaks decreased; this might be attributed the fact that the K^+ ions (0.133 nm) partly replaced the NH_4^+ ions (0.143 nm). Furthermore, the more K^+ doped, the lower the intensity.
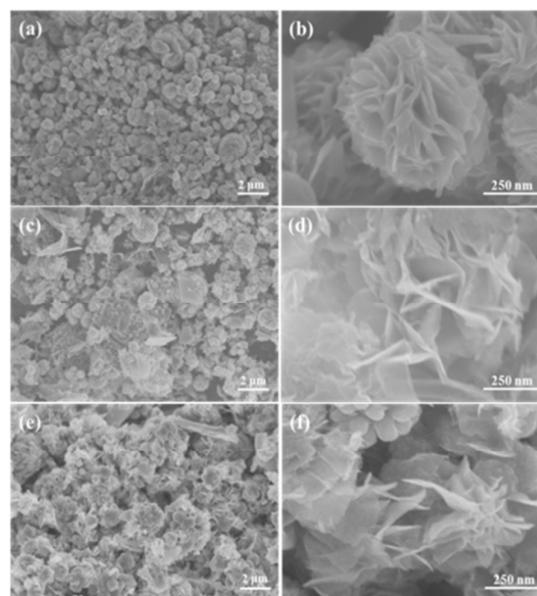

Fig. 2 SEM images of K-doped $(NH_4)_2V_3O_8$/graphene materials (a, b) K-0, (c, d) K-1 and (e, f) K-2.

SEM images of K-0, K-1 and K-2 were depicted in Fig. 2. As presented in Fig. 2a, b, it can be found that a mass of clusters that composed of nanosheets for the sample of K-0. The thickness of these nanosheets is found about 10 nm. Meanwhile, with the increasing the amount of K, the clusters gradually disappear. Moreover, more and more nanosheets appears in K-1 and K-2. This shows that K^+ makes an impact on the morphology of materials. TEM images and HRTEM images are shown in Fig. 3. It can be seen from Fig. 3a, that these clusters have a diameter of about 500 nm. Meanwhile, as presented in 3c and 3e, the lateral sizes of these nanosheets are typically in the ranges of 200 − 500 nm in width and several tens of micrometers in length. As confirmed in Fig. 3b, 3d and 3f, it can be found that their lattice fringe were 0.252, 0.253 and 0.325 nm corresponding to the (311), (311) and (211) interplanar distances of K-0, K-1 and K-2, respectively. In addition, the SAED

patterns in the insets of Fig. 3b, d and f show some diffraction spots which can be indexed to the (001), (211) and (420) planes of the corresponding materials. This is in good agreement with the XRD patterns.
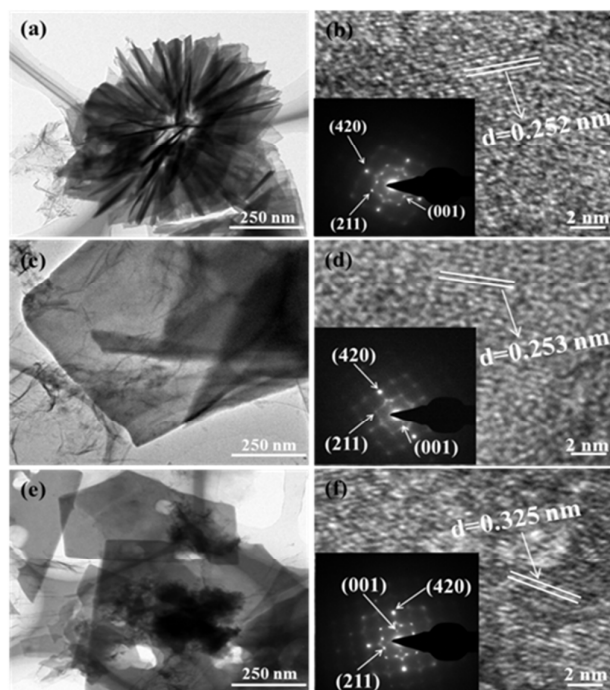

Fig. 3 TEM images of K-doped $(NH_4)_2V_3O_8$/graphene materials (a) K-0, (c) K-1 and (e) K-2; HRTEM images of (b) K-0, (d) K-1 and (f) K-2 (insets: the corresponding SAED patterns).

K-0, K-1 and K-2 structural information is also provided by Raman spectrum in Fig. 4.[42-44] It indicates that K-0, K-1 and K-2 have analogous spectra at 156, 190, 278, 422, 508, 701, 1101, 1350 and 1630 cm^{-1}. The peaks located at 156 and 190 cm^{-1} are assigned to the stretching mode of $(V_2O_2)_n$ corresponding to the chain translation. The lines are strongly associated with the layer structure. Peaks which located at 278 and 422 cm^{-1} are assigned to the vibrations of the O=V bonds. The lines at 508 and 701 cm^{-1} are the V_3-O and V_2-O vibration.[45] The 1101 cm^{-1} line is accounted for the terminal oxygen (V=O) stretching vibration which caused by unshared oxygen.[46] So the results demonstrates that all the samples have the $[V_3O_8]$ layer stack structure. The peaks at 1350 and 1630 cm^{-1} are characteristic peaks of graphene which were assigned as D band and G band, respectively. Usually the D band corresponds to a k-point phonon of A_{1g} symmetry. Simultaneously, the G band is related to the in-plane bond stretching motion of pairs in sp^2 carbon atoms.[47] At the same time, the intensity of D and G band can be used to identify the reaction of graphene.[48] The ratio of I_D to I_G is 0.904 for the pure graphene and 1.06, 1.03 and 1.12 are for K-0, K-1 and K-2 (Fig. S2), respectively. It indicates that the pure graphene has been reduced after hydrothermal process. This is consistent with the previous reports.[49]

The samples are analyzed by XPS (X-ray photoelectron spectroscopy) measurement in Fig. 5. As depicted in Fig. 5a, the survey spectrum reveals that the samples consist of V, O and N on the surface. The 2p core level spectrum of vanadium displays two asymmetrical peaks related to the V $2p_{3/2}$ and V $2p_{1/2}$ orbital. Both V $2p_{3/2}$ and V $2p_{1/2}$ are divided in two peaks, corresponding to V^{5+}

(517.7 eV, 525.48 eV) and V^{4+} (516.2 eV, 524.78 eV), which confirms the mixed valence states of V in Fig. 5b.[50-51] The V^{5+}/V^{4+} molar ratio was calculated from the integration of the V 2p peaks. The V^{5+}/V^{4+} ratio of K-0, K-1, K-2 are 2.03, 2.01 and 1.88, respectively, which are closed to the theoretical value for the $V^{5+}:V^{4+}=2:1$ of $(NH_4)_2V_3O_8$. At the same time in Fig. 5c, we could find the two samples contain K except K-0. Beyond that, K is also certified by EDX (Energy Dispersive X-Ray Spectroscopy) in Fig. S3. They all confirm the presence of doping element. Comparing the C1s XPS spectrum of pure graphene and the graphene after reaction, a significant loss of oxygen-containing functional groups indicates the sufficient reduction of graphene during the hydrothermal process (Fig. S4).
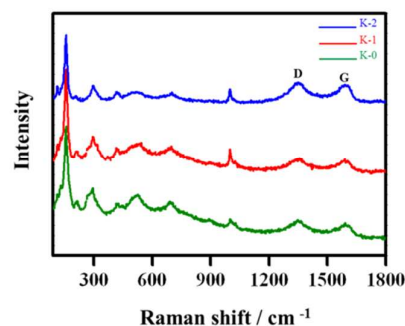

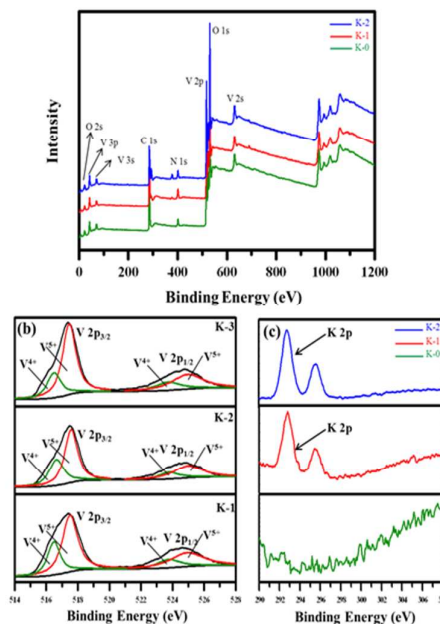**Fig. 4** Raman spectrum of K-doped $(NH_4)_2V_3O_8$/graphene materials.

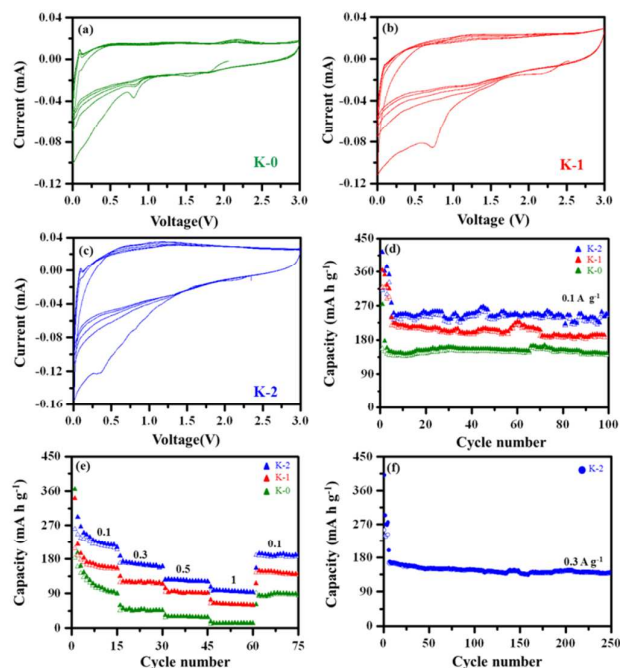**Fig. 5** XPS spectrum of (a) K-doped $(NH_4)_2V_3O_8$/graphene materials, (b) V 2p and (c) K 2p.

Fig. 6 (a-c) CV curves of K-doped $(NH_4)_2V_3O_8$/graphene materials at a scanning rate of 0.5 mV/s in the voltage range of 0.05–3.0 V, respectively; (d) cycling performance of K-doped $(NH_4)_2V_3O_8$/graphene materials at the current rate of 100 mA g^{-1}; (e) rate capabilities from 0.1 to 1 A g^{-1}; (f) cycling performance of K-2 at the current rate of 300 mA g^{-1}.

The electrochemical performance of all the samples is displayed in Fig. 6. In Fig. 6a-c, both the samples' CV curves show a large cathodic peak in the first cycle, owing to the formation of the solid electrolyte interface (SEI) layer. The insertion and extraction of Na ions in K-0, K-1 and K-2 take place in a wide voltage window of 0.05-3V. In Fig. 6d, it can be found that K-0, K-1 and K-2 show high capacities of 144.7, 209.4 and 235.4 mA h g^{-1} at the current density of 100 mA g^{-1} after 100 cycles respectively. The capacity of K-2 is higher than those of K-1 and K-0. Meanwhile, the reduced graphene shows a low capacity at the range of 0.05-3 V and current density of 100 mA g^{-1} (Fig. S5a). At the same time, the rate capability was displayed in Fig. 6e. The capacities of 210, 158.6, 131.9, 93.3 and 190.5 mA h g^{-1} are achieved for K-2 at 0.1, 0.3, 0.5, 1, 0.1 A g^{-1}, respectively. However, K-0 and K-1 displays capacities of 90.2 and 144.5 mA h g^{-1} at the current density of 0.1 mA g^{-1}. K-2 also exhibited the highest rate capability in all samples. The capacity of 142 mA h g^{-1} at the current density of 300 mA g^{-1} after 250 cycles demonstrated that K-2 exhibits good reversibility in Fig. 6f. Furthermore, K-2 displayed long cycling performance in Fig. S5b. After 700 cycles, the retention capacity is 103.2 mA h g^{-1} at the current density of 400 mA g^{-1}. The cycling performance of materials without graphene is shown in Fig. S5c. It can be found that the materials without graphene showed inferior cycling performance at the current density of 100 mA g^{-1}. So the reduced graphene only plays a role in stabilizing the structure. Meanwhile, the capacity of the changed phase $(NH_4)_{1.92}V_3O_8$/graphene is displayed in Fig. S5d. It confirms that excessive K$^+$ restricted the electrochemical properties obviously. So it can be seen that the best doping amount is 10%. In the $(NH_4)_2V_3O_8$, NH$_4^+$ occupies the interlayer site where activation energy is high and NH$_4^+$ cannot emerge. In this system reversible capacity might be from sodiation and desodiation, so
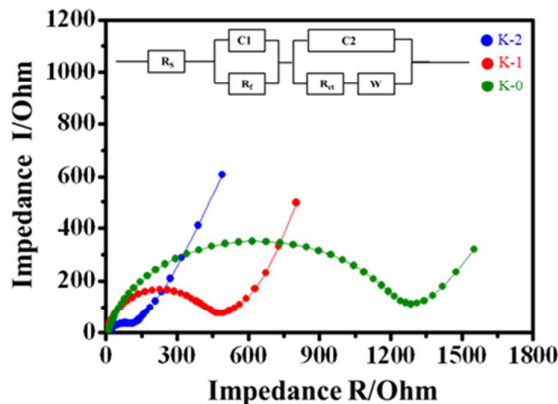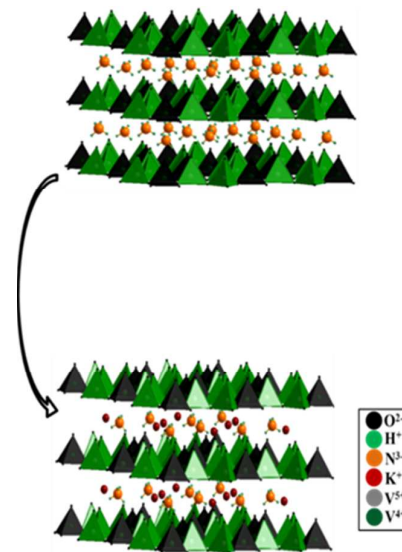

Fig. 7 Nyquist plots of K-doped $(NH_4)_2V_3O_8$/graphene materials.

NH$_4^+$ plays a part in supporting $[V_3O_8]$. Some groups have studied the impacts of metal ion doped layered structure materials.[52-53] It had been found that K$^+$ can improve ammonium vanadates properties. There are two reasons for the improvement of material properties. Firstly, the radius of K$^+$ is smaller than NH$_4^+$ and the space between the layers after the substitution of some NH$_4^+$ can become larger. It's conducive to the transmission of electrons and sodium ions embedded. Finally, the repulsion between Na$^+$ and K$^+$ is smaller than the repulsion between Na$^+$ and NH$_4^+$, so it is benefit for Na$^+$ sodiation and desodiation. So the K-doped $(NH_4)_2V_3O_8$ exhibits good electrochemical properties. Compared with K-doped $Na_6(V_{10}O_{28}).16H_2O^4$, V_2O_5 nano-spheres[5] and $VO_2\cdot1.65H_2O$/graphene microspheres[6], K doped $(NH_4)_2V_3O_8$/graphene shows higher discharge capacity and long cycling times, as shown in Table S1.

Scheme. 1 Schematic illustration of the formation process of K-doped $(NH_4)_2V_3O_8$/graphene.

The electrochemical impedance measurements were performed to elucidate the difference in electrochemical properties. The Nyquist plots for the two samples are one semicircle and a straight sloping line at low frequency in Fig. 7.[54-55] which was fitted by the simplified equivalent circuit in the inset of Fig. 7. The equivalent electrical circuit consists of an active electrolyte resistance R$_S$ in

ARTICLE

series with the parallel combination of the double-layer capacitance C1 and a film capacitance R_f, and the double-layer capacitance C2 and an impedance of a faradaic reaction. In this model, the impedance of a faradaic reaction consists of an active charge transfer resistance R_{ct} and a specific electrochemical element of diffusion W called Warburg element. It can be found that K-2 has smaller charge transfer resistance than K-0 and K-1, which would favour superior capacity and rate performance.

The K-doped $(NH_4)_2V_3O_8$/graphene has a layered structure with more interlayer space, as showed in Scheme. $1,^{56}$ which provide enough space for more Na^+ intercalation and de-intercalation. During the cyclic process, the doped K^+ will act as pillars between layers to help improve the space of the structure. Meanwhile, the repulsive force of Na^+ and K^+ is smaller than the repulsive of Na^+ and NH_4^+. Sodium ions can better intercalate and de-intercalate. Graphene stabilizes the layered structure. Meanwhile, The K-doped $(NH_4)_2V_3O_8$/grapheme (5% and 10%) shown smaller charge transfer resistances, indicating faster electron transfer rate. Therefore, K-doped $(NH_4)_2V_3O_8$/graphene materials can exhibit a better electrochemical performance in sodium-ion batteries.

Conclusions

In summary, we successfully synthesized the K-doped $(NH_4)_2V_3O_8$/graphene materials for the first time. When firstly evaluated as an anode material for sodium-ion batteries, the graphene based K-doped $(NH_4)_2V_3O_8$ composite exhibit high capacity, cycling stability and good rate performance. The improved electrochemical performance might be attributed to two cases. First, the flexible graphene made the structure of $(NH_4)_2V_3O_8$ more stable during repeating sodiation and desodiation. Second, due to the radius of the K^+ is smaller than that of NH_4^+, the K-doped $(NH_4)_2V_3O_8$ owned more interlayer space that benefit for Na^+ movement and faster electron transfer rate. Thus, the graphene based K-doped $(NH_4)_2V_3O_8$ material may be promising as sodium-ion batteries electrode in the future.

Acknowledgements

Notes and references

1 K. Kang, Y. S. Meng, J. Breger, C. P. Grey and G. Ceder, *Science*, 2006, **311**, 977.
2 V. Etacheri, R. Marom, R. Elazari, G. Salitra and D. Aurbach, *Energy Environ. Sci.*, 2011, **4**, 3243.
3 K. Xu, *Chem. Rev.*, 2014, **114**, 11503.
4 L. Zhang, J. Deng , L. Liu, W. Si, S. Oswald, L. Xi, M. Kundu, and G. Ma, T. Gemming, S. Baunack , F. Ding, C. L. Yan and O. G. Schmiddt, *Adv. Mater.*, 2014, **26**, 4527.
5 J. Deng, H. Ji, C. Yan, J. Zhang, W. Si, S. Baunack, S. Oswald, Y. Mei and O. G. Schmidt, *Angew. Chem. Int. Ed.,* 2013, **125**, 2382.
6 W. O. Yah, H. Xu, H. Soejima, W. Ma, Y. Lvov and A. Takahara, *J. Am. Chem. Soc.*, 2012, **134**, 12134.
7 M. V. Reddy, G. V. S. Rao and B. V. R. Chowdari, *Chem. Rev.*, 2013, **113 (7)**, 5364.
8 H. Kim, J. Y. Hong, K. Y. Park, H. Kim, S. W. Kim and K. Kang, *Chem. Rev.*, 2014, **114 (23)**, 11788.
9 A. Manthiram, Y. Z. Fu, S. Heng, C. X. Zu and Y. S. Su, *Chem. Rev.*, 2014, **114 (23)**, 11751.
10 N. A. Yabuuchi, K. Kubota, M. Dahbi, S. C. Komaba. *Chem. Rev.*, 2014, **114**, 11636.
11 M. H. Han, E. Gonzalo, G. Singha and T. Rojo. *Energy. Environ. Sci.*, 2015, **8**, 81.
12 A. Ponrouch, D. Monti, A. Boschin, B. Steen,d P. Johansson, M. R. Palacın. *J. Mater. Chem. A*, 2015, **3**, 22.
13 Y. Y. Kim, K. H. Ha, S. M. Oh and K. TaeLee. *Chem. Eur. J.*, 2014, **20**, 11980.
14 Y. Sun, L. Zhao, H. Pan, X. Lu, L. Gu, Y. S. Hu, H. Li, M. Armand, Y. Ikuhara, L. Chen and X. Huang, *Nat. Commun.*, 2013, **4**, 1870.
15 A. Kohandehghan, K. Cui, M. Kupsta, J. Ding, E. M. Lotfabad, W. P. Kalisvaart and D. Mitlin, *Nano Letters*, 2014, **14**, 5873.
16 Y. Zhu, X. Han, Y. Xu, Y. Liu, S. Zheng, K. Xu, L. Hu and C. Wang, *ACS Nano*, 2013, **7**, 6378.
17 Y. Liu, N. Zhang, L. Jiao, Z. Tao and J. Chen, *Adv. Funct. Mater.*, 2015, **25**, 214.
18 H. G. Wang, Z. Wu, F. L. Meng, D. L. Ma, X. L. Huang, L. M. Wang and X. B. Zhang, *Chem. Sus. Chem.*, 2013, **6**, 56.
19 L. Fu, K. Tang, K. Song, P. A. V. Aken, Y. Yu and J. Maier, *Nanoscale*, 2014, **6**, 1384.
20 Y. Cao, L. Xiao, M. L. Sushko, W. Wang, B. Schwenzer, J. Xiao, Z. Nie, L. V. Saraf, Z. Yang and J. Liu, *Nano Letterts*, 2012, **12**, 3783.
21 W. Wang, B. Jiang, L. W. Hu and Z. S. Lin, *J. Power Sources*, 2014, **250**, 181.
22 C. Nethravathi, C. R. Rajamathi, M. Rajamathi, U. K. Gautam, X. Wang, D. Golberg and Y. Bando, *ACS Appl. Mater. Interfaces*, 2013, **5**, 2708.
23 Q. L. Wei, J. Liu, W. Feng, J. Z. Sheng, X. C. Tian, L. He, Q. Y. An and L. Q. Mai, *J. Mater. Chem. A*, 2015, **3**, 8070.
24 H. L. Fei, X. Liu, Y. S. Lin and M. D. Wei, *J. Colloid and Interface Sci.*, 2014, **428**, 73.
25 H. Y. Wang, K. L. Huang and Y. Ren, *J. Power Sources*, 2011, **196**, 9786.
26 H. L. Fei, H. Li, Z. W. Li, W. J. Feng, X. Liu and M. D. Wei, *Dalton Trans.*, 2014, **43**, 16522.
27 J. Liu, P. J. Lu, S. Q. Liang, J. Liu, W. Wang, M. Lei, S. S. Tang and Q. Yang, *Nano Energy*, 2015, **12**, 709.
28 S. B. Yang, Y. J. Gong, Z. Liu, L. Zhan, D. P. Hashim, L. L. Ma, R. T. Vajtai, and P. M. Ajayan, *Nano Letters*, 2013, **13**, 1596.
29 M. Lee, S. K. Balasingam, H. Y. Jeong, W. G. Hong, H. B. R. Lee, B. H. Kim, Y. Jun, *Sci. Rep.*, 2015, **5**, 8151.
30 G. He, L. J. Li and A. Manthiram, *J. Mater. Chem. A*, 2015, **3**, 14750.
31 H. Yu, X. H. Rui, H. T. Tan, J. Chen, X. Huang, C. Xu, W. L. Liu, D. Y. W. Yu, H. H. Hng and H. E. Hoster, *Nanoscale*, 2013, **5**, 4937.
32 Y. W. Li, J. H. Yao, E. Uchaker, M. Zhang, J. J. Tian, X. Y. Liu and G. Z. Cao, *J. Phys. Chem. C*, 2013, **117**, 23507.
33 J. Y. He, W. M. Wang, Z. G. Zou, F. Long and Z. Y. Fu, *Ionics*, 2014, **20**, 1063.
34 Y. X. Wei, J. Zhou, J. M. Zheng and C. Xu, *Electrochem. Acta*, 2015, **166**, 277.
35 H. Q. Song, Y. G. Liu, C. P. Zhang, C. F. Liu and G. Z. Cao, *J. Mater. Chem. A*, 2015, **3**, 3547.
36 S. Hartung, N. Bucher, H. Y. Chen, A. O. Rammi, S. Sivaramapanicker, B. Parijat, Y. L. Zhao, K. Ulrich, S. Ulrich, H. E. Hoster, and S. Madhavi, *J. Power Sources*, 2015, **288**, 270.
37 D. W. Su, S. X. Dou and G. X. Wang, *ChemSusChem*, 2015, **8**, 2877.
38 S. B. Yang, Y. Sun, L. Chen, Y. Hernandez and X. L. Feng, Müllen, K. *Sci. Rep.*, 2012, **2**, 427.

39 A. Grzechnik, T. Z. Ren, J. M. Possea and K. Friesea, *Dalton Trans.*, 2011, **40**, 4572.
40 T. Z. Ren, Z. Y. Yuan, and X. D. Zou, *Cryst. Res. Technol.*, 2007, **4**, 317.
41 F. R. Theobald and J. G. Theobald, *J. Phys. Chem. Solids*, 1984, **45**, 581.
42 K. Zhu, X. Yan, Y. Zhang, Y. Wang, A. Su, X. Bie, D. Zhang, F. Du and C. Wang, G. Chen, *Chem. Plus Chem.*, 2014, **79**, 447.
43 I. Mjejri, N. Etteyeb and F. Sediri, *Mater. Res. Bull.*, 2013, **48**, 3335.
44 I. Mjejri, N. Etteyeb, F. Sediri, *J. Alloy. Compounds*, 2014, **611**, 372.
45 Q. L. Wei, S. S. Tan, X. Liu and M. Y. Yan, *Adv. Funct. Mater.,* 2015, **25**, 1773.
46 W. Chen, L. Mai, J. Peng, Q. Xu and Q. Zhu, *J. Solid State Chem.*, 2004, **177**, 377.
47 G. Wang, X. Shen, J. Yao and J. Park, *Carbon*, 2009, **47**, 2049.
48 J. Zhu, T. Zhu, X. Zhou, Y. Zhang, X. W. Lou, X. Chen, H. Zhang, H. H. Hng and Q. Yan, *Nanoscale*, 2011, **3**, 1084.
49 P. Wang, Y. Zhai, D. Wang and S. Dong, *Nanoscale*, 2011, **3**, 1640.
50 K. Zhu, X. Yan, Y. Zhang, Y. Wang, A. Su, X. Bie, D. Zhang, F. Du, C. Wang and G. Chen, *Chem. Plus Chem.*, 2014, **79**, 447.
51 M. Simões, Y. Mettan, S. Pokrant and A. Weidenkaff, *J. Phys. Chem. C*, 2014, **118**, 14169.
52 C. Y. Ouyang, D. Y. Wang and S. Q. Shi, *Chin. Phys. Lett.*, 2006, **23**, 61.
53 X. C. Yin, K. L. Huang and S. Liu, *J. Power Sources*, 2010, **195**, 4308.
54 H. L. Fei, X. Liu, H. Li and M. D. Wei. *J. Colloid and Interface Sci.*, 2014, **418**, 273.
55 S. Li, J. X. Qiu, C. Lai, M. Ling, H. J. Zhao and S. Q. Zhang, *Nano Energy*, 2015, **12**, 224.
56 A. Grzechnik, T. Z. Ren, Jose. M. Possea and K. Friesea, *Dalton Trans.*, 2011, **40**, 4572.
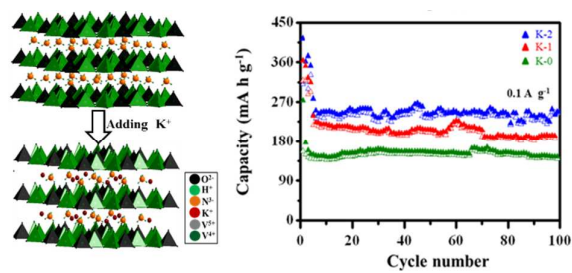
The K-doped $(NH_4)_2V_3O_8$/graphene electrode exhibited stable cycling and good rate performance.